ACS APPLIED NANO MATERIALS

www.acsanm.org Article

Multicolor Fluorescent Graphene Oxide Quantum Dots for Sensing Cancer Cell Biomarkers

Lisandro Cunci,* Viviana González-Colón, Brenda Lee Vargas-Pérez, Joed Ortiz-Santiago, Miraida Pagán, Paola Carrion, Jomari Cruz, Agustin Molina-Ontoria, Namyr Martinez, Walter Silva, Luis Echegoyen, and Carlos R. Cabrera

Cite This: *ACS Appl. Nano Mater.* 2021, 4, 211−219 Read Online

ACCESS | Metrics & More | Article Recommendations | Supporting Information

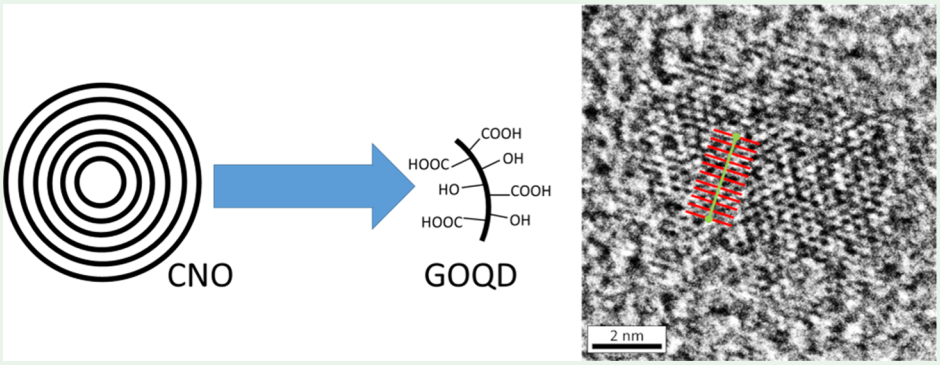

ABSTRACT: Onion-like carbon nanoparticles were synthesized from diamond nanoparticles to be used as the precursor for graphene oxide quantum dots. Onion-like carbon nanoparticles were exfoliated to produce two types of nanoparticles, graphene oxide quantum dots that showed size-dependent fluorescence and highly stable inner cores. Multicolor fluorescent quantum dots were obtained and characterized using different techniques. Polyacrylamide gel electrophoresis showed a range of emission wavelengths spanning from red to blue with the highest intensity shown by green fluorescence. Using high-resolution transmission electron microscopy, we calculated a unit cell size of 2.47 Å in a highly oxidized and defected structure of graphene oxide. A diameter of ca. 4 nm and a radius of gyration of ca. 11 Å were calculated using small-angle X-ray scattering. Finally, the change in fluorescence of the quantum dots was studied when single-stranded DNA that is recognized by telomerase was attached to the quantum dots. Their interaction with the telomerase present in cancer cells was observed and a change was seen after 6 days, providing an important application of these modified graphene oxide quantum dots for cancer sensing.

KEYWORDS: *graphene oxide quantum dots, small-angle X-ray scattering, fluorescence, onion-like carbon nanoparticles, cancer sensing*

INTRODUCTION

Carbon-based quantum dots (graphene oxide quantum dots (GOQDs), graphene quantum dots, and carbon dots) have been synthesized in many different ways that can be grouped into two approaches: top-down[1−4] and bottom-up.[5−7] Top-down approaches mostly use graphite as the starting material, although many others such as carbon nanotubes,[8] XC-72 carbon black,[9] graphite nanofibers,[10] graphite rods,[11] activated charcoal,[12] and even single buckminsterfullerenes have been employed.[13] In the last few years, emphasis has been given in the synthesis of carbon dots[3,14] obtained from coal because of the abundance of this carbon source as studied by Tour et al.[15] Bottom-up approaches use aromatic molecules as starting materials, which are nucleated and grown up to the required size.[3,14,16,17]

GOQDs synthesized from other carbon materials have been vastly studied for many years, due in part to the attention obtained by graphene, a two-dimensional carbon-based material that is only one-atom thick and exhibits outstanding properties scarcely found in other materials. Graphene oxide, however, is obtained through the exfoliation of graphite-like carbon materials, and it consists of a one-atom thick material with the addition of carbon−oxygen moieties that may stand out of the edges and both sides of the basal plane.[18] The oxidation of these carbon-based materials separates the carbon layers, with the addition of oxygen atoms, enough to break van der Waals interactions between them for further exfoliation

Received: September 17, 2020
Accepted: December 11, 2020
Published: December 23, 2020

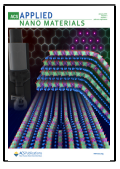

https://dx.doi.org/10.1021/acsanm.0c02526
ACS Appl. Nano Mater. 2021, 4, 211−219

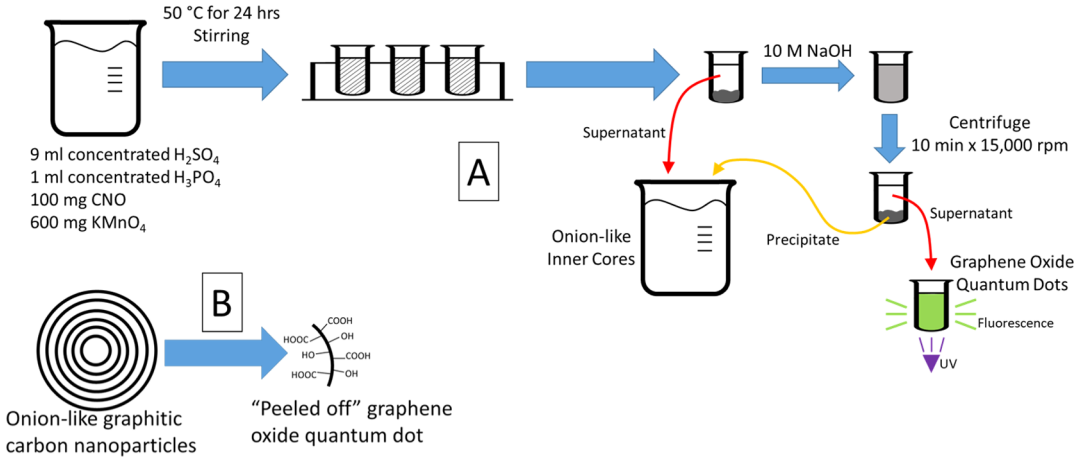

Figure 1. (A) Scheme of the synthesis procedure for GOQDs and (B) summary of the expected results from chemical synthesis.

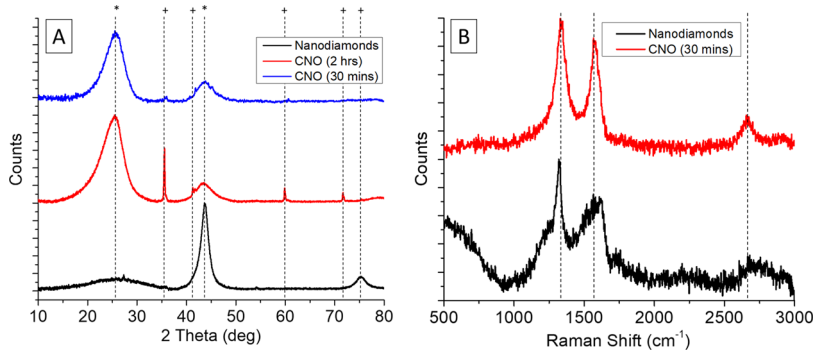

Figure 2. (A) X-ray diffraction of diamond nanoparticles and onion-like carbon nanoparticles processed for 2 h (CNO 2 h) and for 30 min (CNO 30 min) to avoid the formation of silicon carbide. (B) Raman spectroscopy of diamond nanoparticles and onion-like carbon nanoparticles (CNO 30 min).

into separated nanosheets. Because of the strong oxidation procedure, graphene oxide nanosheets are broken down into very small pieces of less than 10−15 nm called GOQDs, which behave as confined spaces for the electrons, exhibiting a new array of properties not shown by graphene oxide. GOQDs have very high solubility in aqueous solutions, while still maintaining areas of the sp^2 structure which allow for the interaction with hydrophobic molecules.[19] GOQDs exhibit fluorescence, and the emitted wavelength depends on their size and degree of oxidation. Carbon-based quantum dots are known to have low quantum yields compared to metal-based quantum dots, with reported values for GOQDs quantum yield as low as 0.4%,[20] with typical values between 7 and 22.9%.[4,16,21−25] Carrier lifetimes have been measured for GOQDs with typical values between 0.45 and 6.98 ns.[26−28] Their fluorescence has been used for different sensing applications such as cell[24] and tumor[29] imaging, bacterial detection,[30] and iron detection,[31] among others. GOQDs have been synthesized from different carbon materials[32] with outstanding properties required for biomedical applications such as biocompatibility. However, GOQDs with only blue and UV fluorescence were synthesized until now using carbon nano-onions (CNO) also called onion-like carbon nanoparticles.[32] In this work, using a stronger oxidation (concentrated sulfuric acid with potassium permanganate) with the use of a second acid (phosphoric acid),[18] we were able to obtain multicolored fluorescent quantum dots, which may be related to the extent of the oxidation of the quantum dots. The generation of a broader spectrum of visible light from GOQDs is important for biological applications and their biocompatibility.

There has been a vast amount of work done in the different types of carbon-based quantum dots with specific applications of GOQDs ranging from metal sensing,[32] cell imaging,[9] and nanofiltration[33] to transistors,[34] among others. In our work, we will be using GOQDs for cancer sensing, specifically telomerase-active cancer, which is 85% of cancer. Using onion-like carbon nanoparticles, we have been able to synthesize GOQDs using an iterative process which progressively "peels off" the layers of the onion-like structures, as shown in Figure 1A. We expected to obtain GOQDs from the graphitic structure of CNO (Figure 1B). GOQDs obtained exhibit fluorescence that depends on the light used for excitation.[35,36] Because of the dependence of the fluorescence of GOQDs on the environment, experiments were conducted to study their use as sensing elements for cancer. Particularly, telomerase was chosen as the biomarker for cancer because of its presence in 85% of cancer and its absence (or negligible concentration) in normal somatic cells.[37,38] After 6 days, we were able to show the use of modified GOQDs using single-stranded DNA that recognizes telomerase as a sensing platform for cancer cells by their change in fluorescence.

RESULTS AND DISCUSSION

Many iterations were carried out for the preparation of CNO from diamonds using the high temperature furnace in which we varied the time at which the diamond nanoparticles were

https://dx.doi.org/10.1021/acsanm.0c02526
ACS Appl. Nano Mater. 2021, 4, 211−219

maintained at 1650 °C. We found that at 2 h, the formation of silicon carbide was carried out, as seen in Figure 2A, with the sharp peaks at ca. 35.5, 41.3, 41.7, 59.9, and 71.7° (+) because of the presence of up to 1000 ppm of silicon dioxide in the diamond nanoparticles that reacted at high temperature to form carbides. The sharpness and height of the peak were due to the structure and size of the silicon carbide nanoparticles formed even though the quantity is very small. After changing the time to 30 min, these peaks disappear with only traces that are removed during the synthesis of GOQDs. The broad peaks that are seen at ca. 25.1 and 43.7° (*) correspond to CNO. The width of the peaks was due to the small size of the nanoparticles according to the Debye−Scherrer equation that states that the smaller the nanoparticle, the broader the peak, because of smaller crystallites. Using the Debye−Scherrer equation for both peaks that correspond to CNO gives us crystallite sizes of 1.7 and 2.1 nm, respectively, while using the same equation for the peaks corresponding to silicon carbide gives ca. 40 nm of crystallite size.

Raman spectroscopy, shown in Figure 2B, was used to characterize and compare the CNO synthesized with the diamond nanoparticles. The spectra of diamond nanoparticles and CNO showed a broader peak at ca. 1320 cm^{-1}, which is related to the defects on the surface of the nanoparticles, called the D peak, as well as a more defined peak at ca. 1600 cm^{-1}, which is related to the graphitic sp^2 structure, which is called the G peak. The presence of the latter peak at the diamond nanoparticles was due to the carbonaceous impurities produced during the synthesis of the diamond, which was lost during the high-temperature synthesis of CNO. In the case of the CNO obtained by the procedure of 30 min, the D and G peaks were located at 1340 cm^{-1} and 1575 cm^{-1}, respectively.[39] These peaks had a small shift from nanodiamonds to CNO toward higher Raman shifts. The D peak represented the A_{1g} vibrational mode which is associated with the sp^3 carbon atoms that are present in defective graphitic areas. The G peak is characteristic of the E_{2g} vibrational mode corresponding to the sp^2 carbon atoms.[39−41] The 2D broad peak is an overtone of the D peak shown between 2550 and 3000 cm^{-1} corresponding to double resonance transitions from the production of two phonons with opposite momentum.[42] At the end, we were able to synthesize reproducible onion-like carbon nanoparticles which were used for the synthesis of GOQDs.

GOQD Synthesis. One of the most important details to have in mind when preparing GOQDs from onion-like carbon nanoparticles is that the byproducts of the synthesis have almost the same size as the GOQDs. This requires additional care to ensure that no other materials that may be deleterious to biological samples stay with the final sample. Therefore, the samples were centrifuged at 15,000 rpm and the supernatant was separated until no precipitate was found. Then, the solution was neutralized using NaOH. The fluorescence was seen using a transilluminator with a 365 nm light, and it was observed that it changed at different pH values. This was expected because graphene oxide is reported to have different functional groups that are protonated at different pH values.[43] This makes the GOQDs aggregate at lower pH, diminishing fluorescence intensity, and makes them separate at higher pH with an increase in fluorescence. The solution also contained high concentration of salts that shields the negativity of the GOQDs and promotes the aggregation, which contributed to the low fluorescence intensity, as can be seen in Figure 3A. In

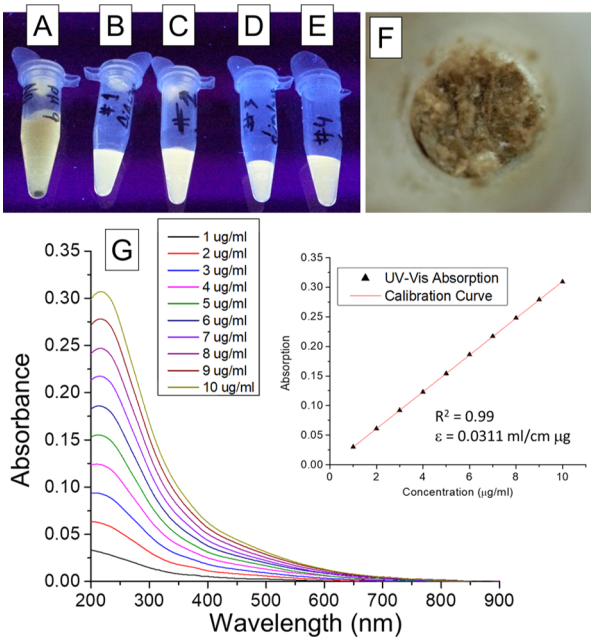

Figure 3. GOQD aliquots obtained (A) before and (B−E) after each day of dialysis excited with UV light (365 nm) in a transilluminator, as well as after (F) lyophilization. (G) UV−vis absorbance measured at different GOQD concentration in water and (insert) calibration curve.

order to purify the samples from the salts, dialysis tube membranes were used. The effect of dialysis is easily observable from the fluorescence of the samples, in Figure 3. An aliquot of the sample, after each day of dialysis, was observed using a transilluminator with a 365 nm light. The change in fluorescence is obvious after the first day of dialysis (Figure 3B) and it becomes less notable in the following days (Figure 3C−E) because the intensity seems to stay the same. Different dialysis membranes were tested starting from 100 kDa and decreasing the pore sizes; however, the 5 kDa membrane was the one with the biggest pore that did not decrease the fluorescence of the sample noticeably after 4 days.

After dialysis, two methods were tried to dry the sample to obtain GOQDs in powder form, using vacuum alone and using lyophilization. Using vacuum alone, most of the solution was evaporated until the concentration was high enough for the intermolecular forces between GOQDs and water to stop the drying process, at which point the water evaporation stopped. A highly concentrated solution of GOQDs was obtained without further drying. Using lyophilization, however, the samples were easily dried after freezing them with liquid nitrogen. Powdered GOQDs after lyophilization are shown in Figure 3F.

Once GOQD samples were obtained in powder, they were weighted and dissolved in nanopure water at a concentration of 1 mg/mL. Using UV−vis absorption spectroscopy, shown in Figure 3G, a calibration curve was obtained (R^2 = 0.99) with concentrations ranging from 1 to 10 μg/mL (Figure 3G, insert) and using the absorption peak at 226 nm. The extinction coefficient was found to be ε = 0.0311 mL/cm μg using Beer−Lambert's Law. UV−vis absorption spectroscopy showed two peaks, one very intense at 226 nm that corresponds to the $\pi \rightarrow \pi^*$ transition of C═C bonds with hybridization sp^2, and a shoulder at 270 nm due to the $n \rightarrow \pi^*$ transition of C═O bonds.[35,36]

https://dx.doi.org/10.1021/acsanm.0c02526
ACS Appl. Nano Mater. 2021, 4, 211−219

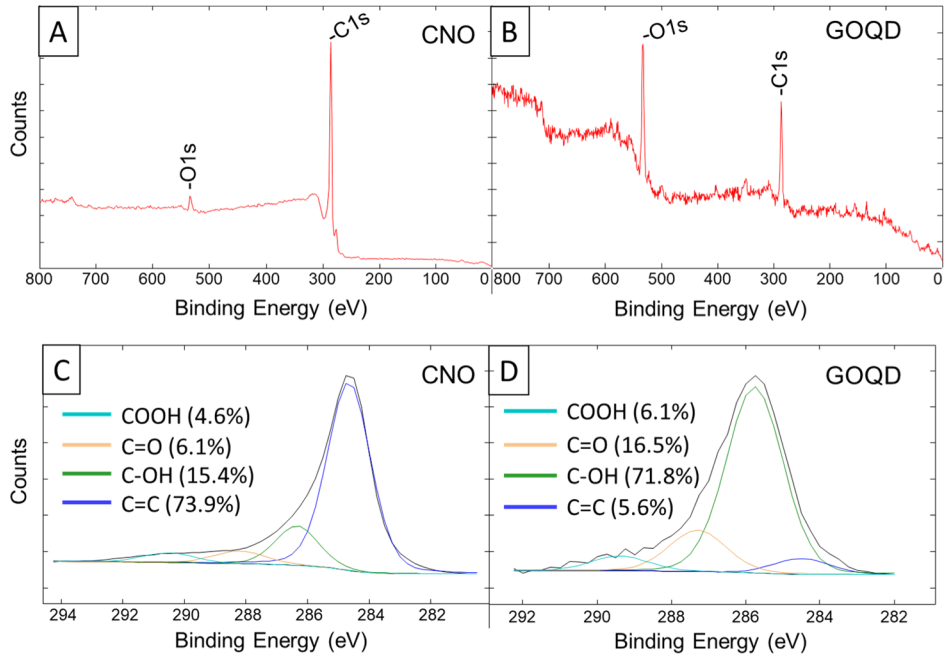

Figure 4. X-ray photoelectron spectra of (B) onion-like carbon nanoparticles (CNO) and (C) GOQDs.

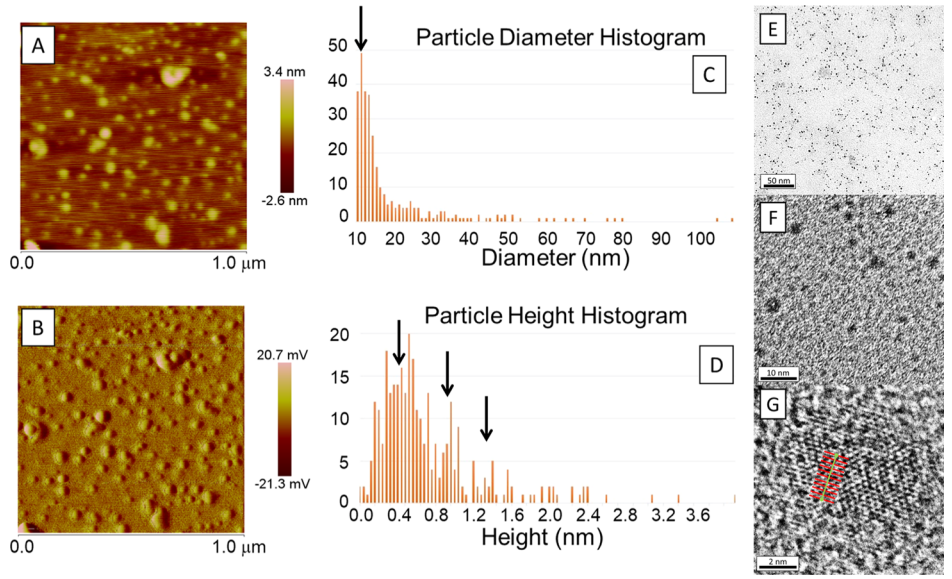

Figure 5. AFM images of (A) height and (B) amplitude. (C) Particle diameter and (D) particle height histograms showing peaks centered on 12 and 0.4 nm, respectively. GOQDs seen using HRTEM at (E) low magnification, (F) medium magnification, and (G) high magnification with unit cell measurements. Black arrows represent the peaks seen in each histogram.

X-ray photoelectron spectroscopy (XPS) was used to compare CNO with GOQDs as shown in Figure 4. Figure 4A,B show the entire spectra of CNO and GOQDs, respectively, with only the carbon 1s and oxygen 1s peaks. It is clearly seen that the oxygen peak is much higher in the GOQD spectrum compared to CNO, which is due to the highly oxidative synthesis used to prepare GOQDs. This was also seen in the carbon 1s peak as shown in Figure 4C,D. The carbon 1s peaks show the difference in hybridization of the carbon atoms after the highly oxidative process to produce GOQDs. The XPS spectrum of CNO (Figure 4C) showed a high atomic proportion (73.9%) of carbon sp^2 with a peak at a binding energy of 284.51 eV, which was contrasted to the proportion found in GOQDs (5.6%), which was much lower due to the high oxidized procedure used for the synthesis. On the other hand, the proportion of the carbon-oxygen moieties found in GOQDs (Figure 4D) is much higher (94.4%) compared to the proportion in CNO (26.1%). Taking into account the error in this technique when used for atomic proportion measurement, the change in carbon moieties proportion is high enough to understand the important change produced by the synthesis in the final structure of GOQDs. Comparing the GOQDs obtained in this work with previously published GOQDs from CNO,[32] we hypothesize that the higher extent of oxidation produced by our synthesis and confirmed with XPS (Figure 4D) influenced the generation of the wide spectrum of emitted multicolored visible light.

https://dx.doi.org/10.1021/acsanm.0c02526
ACS Appl. Nano Mater. 2021, 4, 211−219

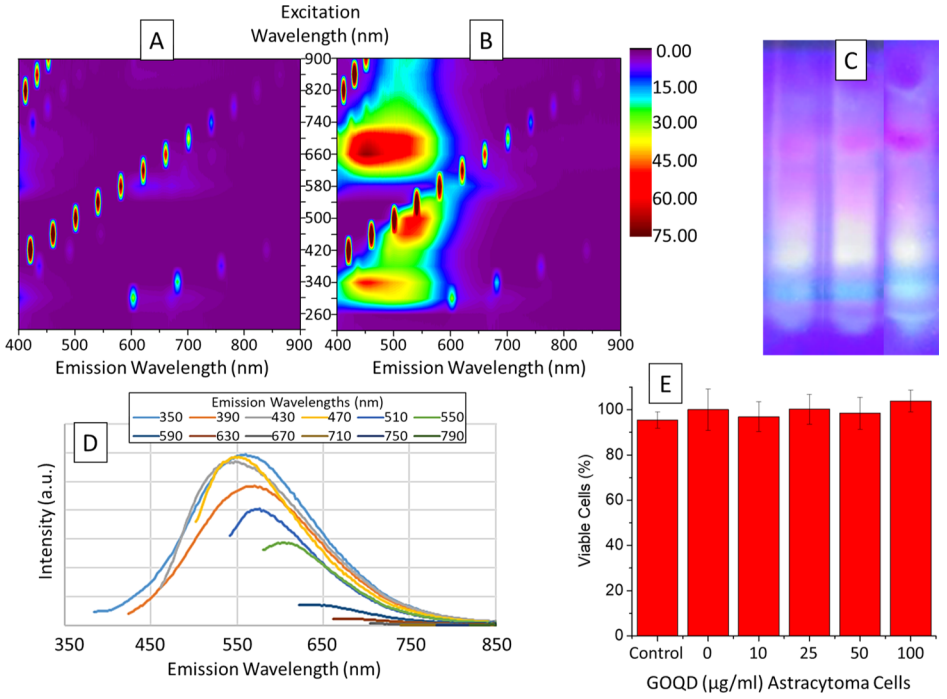

Figure 6. Fluorescence emission maps of (A) water as a baseline and (B) GOQDs in water. (C) Multicolor fluorescence emitted by GOQDs in polyacrylamide gel with an excitation wavelength of 365 nm. (D) Excitation-dependent fluorescence emission of GOQDs and (E) cell viability experiment using MTT colorimetric assay for quantum dot exposure during 1 day to astrocytoma cells.

Atomic force microscopy (AFM) was used to investigate the size of the GOQDs as shown in Figure 5A–D. Figure 5A,B shows the height and amplitude, respectively, of the GOQDs when placed on mica. The size of the images was 1 μm by 1 μm with a color scale for the height between −2.6 and 3.4 nm, and for the amplitude between −21.3 and 20.7 mV. Figure 5C shows the histogram of particle diameter with a peak at 12 nm shown by a black arrow. Additionally, Figure 5D shows the histogram of particle height with the main peak at ca. 0.4 nm, which is consistent with single layer GOQDs, with additional smaller peaks at ca. 0.9 nm and ca. 1.3 nm, indicated by black arrows, consistent with dual and triple layered quantum dots.

GOQDs were found to have less than 10 nm as seen by the high resolution transmission electron microscopy (HRTEM) images in Figure 5E–G, at different magnifications. Figure 5E shows GOQDs as back dots evenly spaced in the holey carbon grid, Figure 5F shows the GOQDs at higher magnification with a size smaller than 10 nm as was expected given that CNOs are known to be less than 10 nm diameter. Figure 5G is showing a GOQDs at high magnification and high resolution where the structure of graphene oxide is clearly seen. The unit cell was calculated using an average of 10 unit cells measured as shown in red and green lines in Figure 5G, with an average of 2.47 Å which is in agreement with the literature.[44] Differently to other reports in the literature,[45] these GOQDs are highly oxidized and defected as seen in their structure observed in the HRTEM. The size of these nanoparticles allows the electrons to behave as in a quantum space, which makes the quantum dots exhibit fluorescence.

Fluorescence of GOQDs. Normally, fluorescence is seen when a high energy photon is used to excite the material such as UV light, and the fluorescence is emitted in with a lower energy such as visible light. In GOQDs, we have measured the fluorescence in a range of wavelengths, and we have found something that seems like upconversion fluorescence and has been reported in the literature as such.[46−49] Moreover, they are reported with the intensity as high as the fluorescence even though it is known that the probability of two-photon fluorescence is much lower.[47,48] We have to be careful to make sure that it is understood that what seems like upconversion fluorescence when using a xenon lamp is due to the second order of the excitation monochromator and has been explained in different published papers.[50−52] However, there are still papers being published after these clarifications using xenon lamp based fluorescent instrumentation to measure and claiming upconversion fluorescence.[47,48] According to the published literature that take the precautions to make sure that upconversion fluorescence is real, only using high power pulsed lasers very low intensity upconversion fluorescence can be observed in GOQDs.[51]

Figure 6A,B show the fluorescence of water and GOQD solution, respectively. Figure 6A shows the fluorescence with only water to use as a baseline and the peaks seen are due to the water, artifacts, the excitation light, and the overtones. Figure 6B shows the fluorescence exhibited by GOQDs where the Y axis shows the wavelength used to excite the quantum dots, and the X axis shows the wavelength emitted by the quantum dots. It is important to clarify the lack of upconversion fluorescence seen with common desktop spectrophotometers because it may be tempting to think that the fluorescence seen in the upper-left quadrant of Figure 6B could be due to this two-photon process. GOQDs synthesized by this method exhibited fluorescence between 400 and 600 nm when excited with wavelengths between 260 and 540 nm. Moreover, the same fluorescence is again seen due to the second order signal in the upper-left quadrant.

Once the synthesis was successful, we hypothesized that different sizes of GOQDs were present with different fluorescence emission wavelengths because of the formation of the fluorescence peaks seen in Figure 6B. In order to

https://dx.doi.org/10.1021/acsanm.0c02526
ACS Appl. Nano Mater. 2021, 4, 211−219

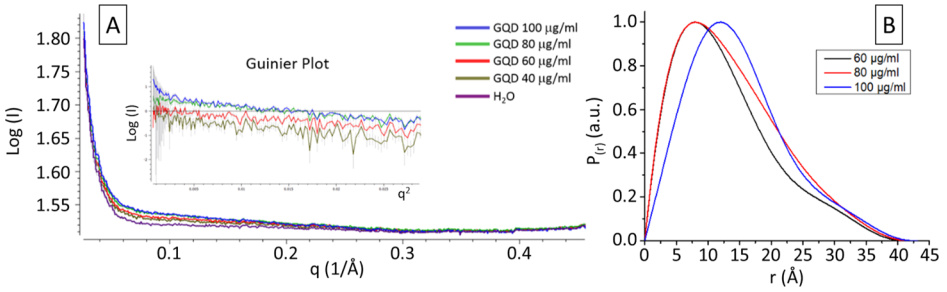

Figure 7. (A) Small-angle X-ray scattering data for different concentrations of GOQDs and nanopure water. (A, inset) Guinier plot for calculation of radius of gyration (R_g) and $I_{(0)}$, which showed agglomeration at a high concentration. (B) Pair distance distribution function ($P_{(r)}$) showing a change in peak position and width, with little or no change in D_{max}. This behavior can be attributed to the agglomeration of nanosheets at high concentrations.

understand the composition of the sizes of our quantum dots to provide these shifting peaks, we performed polyacrylamide gel electrophoresis (PAGE) to separate them by charge and size. These quantum dots are negatively charged at neutral pH, which made them perfect for this separation technique. Agarose gel could not be used because of the small size of the quantum dots in order to have a good separation. Figure 6C shows the 20% PAGE of three samples of GOQDs after applying 100 V for 2 h on a transilluminator with 365 nm UV lamps. The quantum dots separated in a continuum of different sizes with different wavelengths emitted by the different sizes. As it was expected and in agreement with the literature,[3] the smaller quantum dots are lower in the gel and emitted blue fluorescence, and the bigger the quantum dot, the higher the presence in the gel and the higher the wavelength emitted, therefore showing a dependence of the wavelength emitted to the size of the GOQD. Figure 6D confirms the appearance of different sizes of GOQDs by having different emission peaks when using different excitation wavelengths with a decrease in intensity because of the lower amount of GOQDs excited according to the concentrations of each of the different sizes. This effect has been seen in the synthesis of graphene-based quantum dots.[53]

Once the GOQDs were characterized, the cytotoxicity in astrocytoma Cells was investigated using the MTT proliferation assay, which is a colorimetric assay used to study the cell metabolic activity, and correlated to the viability as seen in Figure 6E. In this experiment, astrocytoma cells were exposed to GOQDs for 1 day except for the control in which nothing was added, and the 0 μg/mL that only water was added. The experiments were carried out in triplicate, and the standard deviation is seen in the error bars. As can be clearly seen in these results, there is no effect on the cytotoxicity up to 100 μg/mL.

SAXS Characterization. GOQDs were studied by small-angle X-ray scattering (SAXS) in MacCHESS,[54−56] F1 line, at different concentrations in water from 100 to 40 μg/mL. Graphene oxide nanosheets in nanopure water have more than half of their functional groups protonated,[43] which promotes agglomerations at high concentration. Moreover, SAXS intensity for GOQDs is low because of their small size, creating a compromise where the concentration must be high enough to have reliable data while avoiding agglomeration. Figure 7 shows a $\log(I)-q$ SAXS plot of water and GOQDs at different concentrations.[57] The Guinier plot, after background subtraction, is shown as an inset, and it was used for assessing agglomeration.[58] At low q^2, the data points are increased in 100 μg/mL, showing aggregation of quantum dots, which is decreased at lower concentrations. Using the slope, the radius of gyration (R_g) was calculated at each concentration and is shown in Table 1. At 100 and 80 μg/mL, R_g appears to be higher because of aggregation of quantum dots, compared to 60 μg/mL and 40 μg/mL, which show a smaller R_g. These GOQDs are expected to be curved because of some five-carbon rings which come from the fullerene-like structure of the exfoliated shells of CNO. However, the small curvature and size make them almost disk-shaped, shown by the long linear region seen also at low q^2 in the Guinier plot.

Table 1. Results for GOQDs Obtained by SAXS

concentration (μg/mL)	D_{max} (Å)	R_g (SD) (Å) Guinier method	$I_{(0)}$ (SD) (Å) Guinier method	R_g (SD) (Å) $P_{(r)}$ Method	$I_{(0)}$ (SD) (Å) $P_{(r)}$ Method
40[a]	39.56	9.82 (0.73)	0.78 (0.04)	10.99 (0.68)	0.79 (0.37)
60	41.62	8.93 (0.50)	1.05 (0.03)	10.58 (0.77)	1.10 (0.42)
80	42.26	10.31 (0.52)	1.65 (0.04)	11.19 (0.47)	1.69 (0.42)
100	43.12	11.34 (0.43)	1.87 (0.05)	11.76 (0.37)	1.88 (0.42)

[a]Fluorescence change with telomerase.

The pair distance distribution function ($P_{(r)}$), in Figure 7, shows the difference between agglomerations at different concentrations clearly. It is noteworthy that at 40 μg/mL, the quality of data decreases vastly, making it difficult to obtain a reliable $P_{(r)}$ curve. Assuming that GOQDs agglomerate piling one on top of the other, D_{max}, the diameter of the quantum dots, almost does not change with concentration. However, the position of the peak in $P_{(r)}$ and the width changed because of the increased thickness generated by agglomeration. D_{max} was obtained as ca. 4 nm, which correlates with the literature for the average size of GOQDs with blue-green fluorescence.[10] Using $P_{(r)}$, we calculated R_g in the real space by integrating r^2 over all the pair distance distribution functions and obtained a value of ca. 11 Å, which confirms the approximation carried out by the Guinier plot. R_g and $I_{(0)}$ calculated at each concentration by the different methods are shown in Table 1.

After the synthesis, characterization, and biocompatibility testing of GOQDs, we hypothesized that their fluorescence may be modified with different molecules interacting on their surface. This would provide an optical indication that may be used for sensing. Therefore, we designed an experiment to make a proof-of-concept that would show the change in

https://dx.doi.org/10.1021/acsanm.0c02526
ACS Appl. Nano Mater. 2021, 4, 211−219

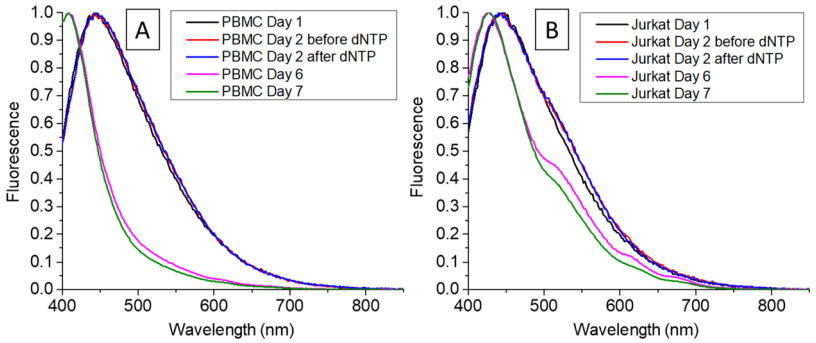

Figure 8. Fluorescence of GOQDs in nuclear extracts of (a) PBMCs and (b) Jurkat cells at different times.

fluorescence produced by the interaction of GOQDs with single-stranded DNA of different sizes attached to their surface that was elongated by telomerase. Telomerase is an enzyme that is present in 85% of cancer which has been the object of study of different sensors in the last few years to detect cancer.[37,59]

In order to show the change in fluorescence of GOQDs in their interaction with telomerase as a biomarker for cancer, single-stranded DNA (ssDNA) probes were tethered to the surface of the quantum dots that include the sequence 5′-TTAGGG-3′ at the end, which is known to be recognized by the enzyme telomerase to elongate the strand repeating the same sequence.[37] Using nuclear extracts from T-cells, cancer-positive (Jurkat cells) and -negative (PBMC) samples were tested, finding that the presence of this enzyme changed the fluorescence of the quantum dots, as can be seen in Figure 8.

Based on these results, it was hypothesized that the change in emission wavelength of the fluorescence emitted by GOQD-DNA when illuminated with UV light is due to the elongation of the telomere-like probe on the surface of the quantum dots. It has been reported that ssDNA has affinity toward the nonpolar areas of the graphene oxide interacting noncovalently by intermolecular forces.[60,61] Double-stranded DNA, however, cannot bind to GOQDs because of the helix formation.

CONCLUSIONS

GOQDs have been synthesized from CNO by oxidation and exfoliation of their atomic layers. Raman and XRD characterization showed the confirmation of their synthesis, while avoiding the formation of silicon carbide. After purification, the synthesis produced a wide range of sizes of GOQDs that had different emission wavelengths. The shift in the emission peak was seen with the excitation wavelength, and PAGE was used to show the difference in fluorescence at different sizes. The radius of gyration of GOQDs was calculated using SAXS, and both the pair distribution function and the Guinier plot produced a similar value of ca. 11.5 Å. Moreover, D_{max} was found to be ca. 4 nm, which increased with concentration because of agglomeration of GOQDs. Given the biocompatibility of GOQDs, they were used as fluorescent probes by modifying them with single-stranded DNA designed to be elongated by telomerase. The change in fluorescence with time was measured when telomerase is present in cancerous versus noncancerous T-cell nuclear extracts. Several clear emission peaks were found after 6 and 7 days in the presence of telomerase that were not seen in noncancerous cells. In this way, we were able to show the novel application of using modified GOQDs for telomerase-positive cancer sensing by exploiting their change in fluorescence when interacting with telomerase.

ASSOCIATED CONTENT

Supporting Information

The Supporting Information is available free of charge at https://pubs.acs.org/doi/10.1021/acsanm.0c02526.

CNO and GOQD syntheses and purification (PDF)

AUTHOR INFORMATION

Corresponding Author

Lisandro Cunci − *Department of Chemistry, Universidad Ana G. Méndez, Gurabo, Puerto Rico 00778, United States;* orcid.org/0000-0002-7315-177X; Phone: +1-787-743-7979 x9-4744; Email: cuncil1@uagm.edu; Fax: +1-787-743-4114

Authors

Viviana González-Colón − *Department of Physiology, University of Puerto Rico Medical Sciences Campus, San Juan, Puerto Rico 00936, United States*

Brenda Lee Vargas-Pérez − *Department of Chemistry, Universidad Ana G. Méndez, Gurabo, Puerto Rico 00778, United States*

Joed Ortiz-Santiago − *Department of Chemistry, Universidad Ana G. Méndez, Gurabo, Puerto Rico 00778, United States*

Miraida Pagán − *Department of Chemistry, Universidad Ana G. Méndez, Gurabo, Puerto Rico 00778, United States*

Paola Carrion − *Department of Chemistry, Universidad Ana G. Méndez, Gurabo, Puerto Rico 00778, United States*

Jomari Cruz − *Department of Chemistry, Universidad Ana G. Méndez, Gurabo, Puerto Rico 00778, United States*

Agustin Molina-Ontoria − *IMDEA-Nanociencia, Madrid 28049, Spain;* orcid.org/0000-0003-3924-7150

Namyr Martinez − *Department of Physiology, University of Puerto Rico Medical Sciences Campus, San Juan, Puerto Rico 00936, United States*

Walter Silva − *Department of Physiology, University of Puerto Rico Medical Sciences Campus, San Juan, Puerto Rico 00936, United States*

Luis Echegoyen − *Department of Chemistry, University of Texas at El Paso, El Paso, Texas 79968, United States;* orcid.org/0000-0003-1107-9423

Carlos R. Cabrera − *Department of Chemistry, University of Puerto Rico Rio Piedras Campus, San Juan, Puerto Rico 00925, United States;* orcid.org/0000-0002-3342-8666

Complete contact information is available at: https://pubs.acs.org/10.1021/acsanm.0c02526

https://dx.doi.org/10.1021/acsanm.0c02526
ACS Appl. Nano Mater. 2021, 4, 211−219

Notes

The authors declare no competing financial interest.

■ ACKNOWLEDGMENTS

This project was supported by an Institutional Development Award (IDeA) from the National Institute of General Medical Sciences of the National Institutes of Health under grant number P20 GM103475-14, the National Science Foundation under award numbers 1827622 and 1849243, and the Puerto Rico Science, Technology, and Research Trust award number 2016-00068. This content is only the responsibility of the authors and does not necessarily represent the official views of the National Institutes of Health, the National Science Foundation, or the Puerto Rico Science, Technology, and Research Trust. The authors acknowledge the Puerto Energy Center at Universidad Ana G. Mendez − Gurabo Campus and Ian Gutierrez for the use of the X-ray diffraction facilities and the Molecular Science Research Center (MSRC) at the University of Puerto Rico for the use of the Raman spectroscopy facilities. The authors acknowledge Dr. Valance Washington from the Department of Biology at the University of Puerto Rico, Rio Piedras Campus, for the blood sample. The authors also acknowledge Dr. Angel Marti from Rice University for scientific chats related to the possibility of upconversion fluorescence in GOQDs. Authors acknowledge Dr. Gillilan at MacCHESS for his help in carrying out the analysis of the samples. This work is based upon research conducted at the Cornell High Energy Synchrotron Source (CHESS), which is supported by the National Science Foundation and the National Institutes of Health/National Institute of General Medical Sciences under NSF award DMR-1829070, using the Macromolecular Diffraction at CHESS (MacCHESS) facility, which is supported by award GM-124166 from the National Institutes of Health, through its National Institute of General Medical Sciences.

■ REFERENCES

(1) Qin, Y.; Cheng, Y.; Jiang, L.; Jin, X.; Li, M.; Luo, X.; Liao, G.; Wei, T.; Li, Q. Top-down Strategy toward Versatile Graphene Quantum Dots for Organic/Inorganic Hybrid Solar Cells. *ACS Sustain. Chem. Eng.* **2015**, *3*, 637−644.

(2) Hu, H.; Quan, H.; Zhong, B.; Li, Z.; Huang, Y.; Wang, X.; Zhang, M.; Chen, D. A Reduced Graphene Oxide Quantum Dot-Based Adsorbent for Efficiently Binding with Organic Pollutants. *ACS Appl. Nano Mater.* **2018**, *1*, 6502−6513.

(3) Ye, R.; Peng, Z.; Metzger, A.; Lin, J.; Mann, J. A.; Huang, K.; Xiang, C.; Fan, X.; Samuel, E. L. G.; Alemany, L. B.; Martí, A. A.; Tour, J. M. Bandgap engineering of coal-derived graphene quantum dots. *ACS Appl. Mater. Interfaces* **2015**, *7*, 7041−7048.

(4) Yoon, H.; Kim, H. S.; Kim, J.; Park, M.; Kim, B.; Lee, S.; Kang, K.; Yoo, S.; Jeon, S. Blue Graphene Quantum Dots with High Color Purity by Controlling Subdomain Formation for Light-Emitting Devices. *ACS Appl. Nano Mater.* **2020**, *3*, 6469−6477.

(5) Gao, T.; Wang, X.; Zhao, J.; Jiang, P.; Jiang, F.-L.; Liu, Y. Bridge between Temperature and Light: Bottom-Up Synthetic Route to Structure-Defined Graphene Quantum Dots as a Temperature Probe In Vitro and in Cells. *ACS Appl. Mater. Interfaces* **2020**, *12*, 22002−22011.

(6) Liu, R.; Wu, D.; Feng, X.; Müllen, K. Bottom-up fabrication of photoluminescent graphene quantum dots with uniform morphology. *J. Am. Chem. Soc.* **2011**, *133*, 15221−15223.

(7) Mueller, M. L.; Yan, X.; Dragnea, B.; Li, L.-s. Slow hot-carrier relaxation in colloidal graphene quantum dots. *Nano Lett.* **2011**, *11*, 56−60.

(8) Wei, S.; Zhang, R.; Liu, Y.; Ding, H.; Zhang, Y.-L. Graphene quantum dots prepared from chemical exfoliation of multiwall carbon nanotubes: An efficient photocatalyst promoter. *Catal. Commun.* **2016**, *74*, 104−109.

(9) Hong, G.-L.; Zhao, H.-L.; Deng, H.-H.; Yang, H.-J.; Peng, H.-P.; Liu, Y.-H.; Chen, W. Fabrication of ultra-small monolayer graphene quantum dots by pyrolysis of trisodium citrate for fluorescent cell imaging. *Int. J. Nanomed.* **2018**, *13*, 4807−4815.

(10) Peng, J.; Gao, W.; Gupta, B. K.; Liu, Z.; Romero-Aburto, R.; Ge, L.; Song, L.; Alemany, L. B.; Zhan, X.; Gao, G.; Vithayathil, S. A.; Kaipparettu, B. A.; Marti, A. A.; Hayashi, T.; Zhu, J.-J.; Ajayan, P. M. Graphene Quantum Dots Derived from Carbon Fibers. *Nano Lett.* **2012**, *12*, 844−849.

(11) Ahirwar, S.; Mallick, S.; Bahadur, D. Electrochemical Method To Prepare Graphene Quantum Dots and Graphene Oxide Quantum Dots. *ACS Omega* **2017**, *2*, 8343−8353.

(12) Dong, Y.; Zhou, N.; Lin, X.; Lin, J.; Chi, Y.; Chen, G. Extraction of Electrochemiluminescent Oxidized Carbon Quantum Dots from Activated Carbon. *Chem. Mater.* **2010**, *22*, 5895−5899.

(13) Chua, C. K.; Sofer, Z.; Šimek, P.; Jankovský, O.; Klímová, K.; Bakardjieva, S.; Hrdličková Kučková, Š.; Pumera, M. Synthesis of strongly fluorescent graphene quantum dots by cage-opening buckminsterfullerene. *ACS Nano* **2015**, *9*, 2548−2555.

(14) Nilewski, L.; Mendoza, K.; Jalilov, A. S.; Berka, V.; Wu, G.; Sikkema, W. K. A.; Metzger, A.; Ye, R.; Zhang, R.; Luong, D. X.; Wang, T.; McHugh, E.; Derry, P. J.; Samuel, E. L.; Kent, T. A.; Tsai, A.-L.; Tour, J. M. Highly Oxidized Graphene Quantum Dots from Coal as Efficient Antioxidants. *ACS Appl. Mater. Interfaces* **2019**, *11*, 16815−16821.

(15) Ye, R.; Xiang, C.; Lin, J.; Peng, Z.; Huang, K.; Yan, Z.; Cook, N. P.; Samuel, E. L.; Hwang, C. C.; Ruan, G.; Ceriotti, G.; Raji, A. R.; Marti, A. A.; Tour, J. M. Coal as an abundant source of graphene quantum dots. *Nat. Commun.* **2013**, *4*, 2943.

(16) Li, L.; Wu, G.; Yang, G.; Peng, J.; Zhao, J.; Zhu, J.-J. Focusing on luminescent graphene quantum dots: current status and future perspectives. *Nanoscale* **2013**, *5*, 4015−4039.

(17) Bacon, M.; Bradley, S. J.; Nann, T. Graphene Quantum Dots. *Part. Part. Syst. Charact.* **2014**, *31*, 415−428.

(18) Cunci, L.; Velez, C. A.; Perez, I.; Suleiman, A.; Larios, E.; José-Yacamán, M.; Watkins, J. J.; Cabrera, C. R. Platinum electrodeposition at unsupported electrochemically reduced nanographene oxide for enhanced ammonia oxidation. *ACS Appl. Mater. Interfaces* **2014**, *6*, 2137−2145.

(19) Sun, X.; Liu, Z.; Welsher, K.; Robinson, J. T.; Goodwin, A.; Zaric, S.; Dai, H. Nano-Graphene Oxide for Cellular Imaging and Drug Delivery. *Nano Res.* **2008**, *1*, 203−212.

(20) Shen, S.; Wang, J.; Wu, Z.; Du, Z.; Tang, Z.; Yang, J. Graphene Quantum Dots with High Yield and High Quality Synthesized from Low Cost Precursor of Aphanitic Graphite. *Nanomaterials* **2020**, *10*, 375.

(21) Zhang, M.; Bai, L.; Shang, W.; Xie, W.; Ma, H.; Fu, Y.; Fang, D.; Sun, H.; Fan, L.; Han, M.; Liu, C.; Yang, S. Facile synthesis of water-soluble, highly fluorescent graphene quantum dots as a robust biological label for stem cells. *J. Mater. Chem.* **2012**, *22*, 7461.

(22) Wang, Z.; Yu, J.; Zhang, X.; Li, N.; Liu, B.; Li, Y.; Wang, Y.; Wang, W.; Li, Y.; Zhang, L.; Dissanayake, S.; Suib, S. L.; Sun, L. Large-Scale and Controllable Synthesis of Graphene Quantum Dots from Rice Husk Biomass: A Comprehensive Utilization Strategy. *ACS Appl. Mater. Interfaces* **2016**, *8*, 1434−1439.

(23) Pan, D.; Zhang, J.; Li, Z.; Wu, M. Hydrothermal route for cutting graphene sheets into blue-luminescent graphene quantum dots. *Adv. Mater.* **2010**, *22*, 734−738.

(24) Sun, H.; Wu, L.; Gao, N.; Ren, J.; Qu, X. Improvement of photoluminescence of graphene quantum dots with a biocompatible photochemical reduction pathway and its bioimaging application. *ACS Appl. Mater. Interfaces* **2013**, *5*, 1174−1179.

(25) Tian, P.; Tang, L.; Teng, K. S.; Lau, S. P. Graphene quantum dots from chemistry to applications. *Mater. Today Chem.* **2018**, *10*, 221−258.

https://dx.doi.org/10.1021/acsanm.0c02526
ACS Appl. Nano Mater. 2021, 4, 211−219

(26) Ghosh, T.; Prasad, E. White-Light Emission from Unmodified Graphene Oxide Quantum Dots. *J. Phys. Chem. C* **2015**, *119*, 2733−2742.
(27) Dey, T.; Mukherjee, S.; Ghorai, A.; Das, S.; Ray, S. K. Effects of Size and Localized States in Charge Carrier Dynamics and Performance of Solution-Processed Graphene Quantum Dots/Silicon Heterojunction Near-UV Photodetectors. *J. Phys. Chem. C* **2020**, *124*, 12161−12167.
(28) Chae, W.-S.; Yun, J.; Nam, S.-H.; Lee, S.-G.; Yang, W.-G.; Yoon, H.; Park, M.; Jeon, S. Fluorescence Modulation of Graphene Quantum Dots Near Structured Silver Nanofilms. *ACS Appl. Mater. Interfaces* **2018**, *10*, 14079−14086.
(29) Xu, A.; He, P.; Ye, C.; Liu, Z.; Gu, B.; Gao, B.; Li, Y.; Dong, H.; Chen, D.; Wang, G.; Yang, S.; Ding, G. Polarizing Graphene Quantum Dots toward Long-Acting Intracellular Reactive Oxygen Species Evaluation and Tumor Detection. *ACS Appl. Mater. Interfaces* **2020**, *12*, 10781−10790.
(30) Gao, R.; Zhong, Z.; Gao, X.; Jia, L. Graphene Oxide Quantum Dots Assisted Construction of Fluorescent Aptasensor for Rapid Detection of Pseudomonas aeruginosa in Food Samples. *J. Agric. Food Chem.* **2018**, *66*, 10898−10905.
(31) Kalaiyarasan, G.; Joseph, J.; Kumar, P. Phosphorus-Doped Carbon Quantum Dots as Fluorometric Probes for Iron Detection. *ACS Omega* **2020**, *5*, 22278−22288.
(32) Liu, Y.; Kim, D. Y. Ultraviolet and blue emitting graphene quantum dots synthesized from carbon nano-onions and their comparison for metal ion sensing. *Chem. Commun.* **2015**, *51*, 4176−4179.
(33) Zhang, C.; Wei, K.; Zhang, W.; Bai, Y.; Sun, Y.; Gu, J. Graphene Oxide Quantum Dots Incorporated into a Thin Film Nanocomposite Membrane with High Flux and Antifouling Properties for Low-Pressure Nanofiltration. *ACS Appl. Mater. Interfaces* **2017**, *9*, 11082−11094.
(34) Kim, Y.-H.; Lee, E. Y.; Lee, H. H.; Seo, T. S. Characteristics of Reduced Graphene Oxide Quantum Dots for a Flexible Memory Thin Film Transistor. *ACS Appl. Mater. Interfaces* **2017**, *9*, 16375−16380.
(35) Luo, Z.; Lu, Y.; Somers, L. A.; Johnson, A. T. C. High yield preparation of macroscopic graphene oxide membranes. *J. Am. Chem. Soc.* **2009**, *131*, 898−899.
(36) Shang, J.; Ma, L.; Li, J.; Ai, W.; Yu, T.; Gurzadyan, G. G. The origin of fluorescence from graphene oxide. *Sci. Rep.* **2012**, *2*, 792.
(37) Cunci, L.; Martinez Vargas, M.; Cunci, R.; Gomez-Moreno, R.; Perez, I.; Baerga-Ortiz, A.; Gonzalez, C. I.; Cabrera, C. R. Real-Time Detection of Telomerase Activity in Cancer Cells using a Label-Free Electrochemical Impedimetric Biosensing Microchip. *RSC Adv.* **2014**, *4*, 52357−52365.
(38) Defever, T.; Druet, M.; Rochelet-Dequaire, M.; Joannes, M.; Grossiord, C.; Limoges, B.; Marchal, D. Real-Time Electrochemical Monitoring of the Polymerase Chain Reaction by Mediated Redox Catalysis. *J. Am. Chem. Soc.* **2009**, *131*, 11433−11441.
(39) Ferrari, A. C.; Robertson, J. Interpretation of Raman spectra of disordered and amorphous carbon. *Phys. Rev. B: Condens. Matter Mater. Phys.* **2000**, *61*, 14095−14107.
(40) Shahriary, L.; Athawale, A. A. Graphene Oxide Synthesized by Using Modified Hummers Approach. *Int. J. Renew. Energy Environ. Eng.* **2014**, *2*, 58.
(41) Cuong, T. V.; Pham, V. H.; Tran, Q. T.; Hahn, S. H.; Chung, J. S.; Shin, E. W.; Kim, E. J. Photoluminescence and Raman studies of graphene thin films prepared by reduction of graphene oxide. *Mater. Lett.* **2010**, *64*, 399−401.
(42) Zhao, J.; Liu, L.; Li, F. *Graphene Oxide: Physics and Applications*; Springer, 2015; Vol. *1*.
(43) Konkena, B.; Vasudevan, S. Understanding Aqueous Dispersibility of Graphene Oxide and Reduced Graphene Oxide through pK(a) Measurements. *J. Phys. Chem. Lett.* **2012**, *3*, 867−872.
(44) Yang, G.; Li, L.; Lee, W. B.; Ng, M. C. Structure of graphene and its disorders: a review. *Sci. Technol. Adv. Mater.* **2018**, *19*, 613−648.
(45) Zhu, J.; Tang, Y.; Wang, G.; Mao, J.; Liu, Z.; Sun, T.; Wang, M.; Chen, D.; Yang, Y.; Li, J.; Deng, Y.; Yang, S. Green, Rapid, and Universal Preparation Approach of Graphene Quantum Dots under Ultraviolet Irradiation. *ACS Appl. Mater. Interfaces* **2017**, *9*, 14470−14477.
(46) Zhuo, S.; Shao, M.; Lee, S.-T. Upconversion and down-conversion fluorescent graphene quantum dots: ultrasonic preparation and photocatalysis. *ACS Nano* **2012**, *6*, 1059−1064.
(47) Wu, C.; Chen, R.; Ma, C.; Cheng, R.; Gao, X.; Wang, T.; Liu, Y.; Huo, P.; Yan, Y. Construction of upconversion nitrogen doped graphene quantum dots modified BiVO4 photocatalyst with enhanced visible-light photocatalytic activity. *Ceram. Int.* **2019**, *45*, 2088−2096.
(48) Ke, J.; Li, X.; Zhao, Q.; Liu, B.; Liu, S.; Wang, S. Upconversion carbon quantum dots as visible light responsive component for efficient enhancement of photocatalytic performance. *J. Colloid Interface Sci.* **2017**, *496*, 425−433.
(49) Li, M.; Wu, W.; Ren, W.; Cheng, H.-M.; Tang, N.; Zhong, W.; Du, Y. Synthesis and upconversion luminescence of N-doped graphene quantum dots. *Appl. Phys. Lett.* **2012**, *101*, 103107.
(50) Barati, A.; Shamsipur, M.; Abdollahi, H. A misunderstanding about upconversion luminescence of carbon quantum dots. *J. Iran. Chem. Soc.* **2014**, *12*, 441−446.
(51) Gan, Z.; Wu, X.; Zhou, G.; Shen, J.; Chu, P. K. Is There Real Upconversion Photoluminescence from Graphene Quantum Dots? *Adv. Opt. Mater.* **2013**, *1*, 554−558.
(52) Wen, X.; Yu, P.; Toh, Y.-R.; Ma, X.; Tang, J. On the upconversion fluorescence in carbon nanodots and graphene quantum dots. *Chem. Commun.* **2014**, *50*, 4703−4706.
(53) Zeng, M.; Shah, S. A.; Huang, D.; Parviz, D.; Yu, Y.-H.; Wang, X.; Green, M. J.; Cheng, Z. Aqueous Exfoliation of Graphite into Graphene Assisted by Sulfonyl Graphene Quantum Dots for Photonic Crystal Applications. *ACS Appl. Mater. Interfaces* **2017**, *9*, 30797−30804.
(54) Hopkins, J. B.; Gillilan, R. E.; Skou, S. BioXTAS RAW: improvements to a free open-source program for small-angle X-ray scattering data reduction and analysis. *J. Appl. Crystallogr.* **2017**, *50*, 1545−1553.
(55) Acerbo, A. S.; Cook, M. J.; Gillilan, R. E. Upgrade of MacCHESS facility for X-ray scattering of biological macromolecules in solution. *J. Synchrotron Radiat.* **2015**, *22*, 180−186.
(56) Skou, S.; Gillilan, R. E.; Ando, N. Synchrotron-based small-angle X-ray scattering of proteins in solution. *Nat. Protoc.* **2014**, *9*, 1727−1739.
(57) Konarev, P. V.; Volkov, V. V.; Sokolova, A. V.; Koch, M. H. J.; Svergun, D. I. PRIMUS: a Windows PC-based system for small-angle scattering data analysis. *J. Appl. Crystallogr.* **2003**, *36*, 1277−1282.
(58) Petoukhov, M. V.; Konarev, P. V.; Kikhney, A. G.; Svergun, D. I. ATSAS 2.1 − towards automated and web-supported small-angle scattering data analysis. *J. Appl. Crystallogr.* **2007**, *40*, s223−s228.
(59) Díaz-Cartagena, D. C.; Hernández-Cancel, G.; Bracho-Rincón, D. P.; González-Feliciano, J. A.; Cunci, L.; González, C. I.; Cabrera, C. R. Label-Free Telomerase Activity Detection via Electrochemical Impedance Spectroscopy. *ACS Omega* **2019**, *4*, 16724−16732.
(60) Tang, Z.; Wu, H.; Cort, J. R.; Buchko, G. W.; Zhang, Y.; Shao, Y.; Aksay, I. A.; Liu, J.; Lin, Y. Constraint of DNA on functionalized graphene improves its biostability and specificity. *Small* **2010**, *6*, 1205−1209.
(61) Liu, B.; Salgado, S.; Maheshwari, V.; Liu, J. DNA adsorbed on graphene and graphene oxide: Fundamental interactions, desorption and applications. *Curr. Opin. Colloid Interface Sci.* **2016**, *26*, 41−49.

https://dx.doi.org/10.1021/acsanm.0c02526
ACS Appl. Nano Mater. 2021, 4, 211−219